J Appl Electrochem (2009) 39:2115–2121
DOI 10.1007/s10800-009-9879-1

ORIGINAL PAPER

Nanostructured bimetallic alloys prepared via mechanochemical synthesis as PEMFC electrocatalysts for automotive applications

Mihaela Aneta Dumitrescu · Marialaura Lucariello · Elisabetta Arca · Maela Manzoli · Carlotta Francia · Elisa Paola Ambrosio

Received: 7 October 2008 / Accepted: 19 March 2009 / Published online: 1 April 2009

Abstract Pt–Co alloys prepared by high energy ball milling synthesis were tested as electrocatalysts for hydrogen fueled Polymer Electrolyte Membrane Fuel Cells (PEMFC). In the present contribution we report on the first results regarding the electrochemical behaviour of two samples of Pt–Co alloys. One sample contains 20 wt.% alloy Pt:Co in the molar ratio 0.25:0.75 and C 80 wt.% and the second one Pt:Co in the molar ratio 0.75:0.25 and C 80 wt.%. The electrochemically active surface (EAS) was determined by cyclic voltammetry data while the electrocatalyst performance in a real cell was obtained by assembling Membrane Electrode Assemblies (MEAs) with the considered sample at the cathode. The results obtained, though indicating a lower performance than all-Pt catalysts, are quite interesting as they point out the importance of the C/Pt, Nafion/Pt and Pt/Co ratios that exert a deep influence onto the cell performance.

Keywords PEMFC · MEA · Pt–Co alloys · High energy ball milling · ORR · Electrochemical testing

M. A. Dumitrescu (✉) · C. Francia · E. P. Ambrosio
Department of Materials Science and Chemical Engineering, Politecnico di Torino, Corso Duca degli Abruzzi 24, 10129 Torino, Italy
e-mail: mihaela.dumitrescu@polito.it

M. Lucariello
HySyLab—Hydrogen System Laboratory, Environment Park S.p.A.Via Livorno 60, 10144 Torino, Italy

E. Arca
Università di Sassari, Via Vienna n. 2, 07100 Sassari, Italy

M. Manzoli
Università degli Studi di Torino, Via Pietro Giuria 7, 10125 Torino, Italy

1 Introduction

The rising of oil price during last years, the fossil fuels consumption and the environmental pollution are leading to an ever increasing interest on possible alternative energy sources. The Polymer Electrolyte Membrane Fuel Cell (PEMFC) represents a sound alternative, suitable as a power plant, via a combined electrolyzer/fuel cell system, easily extendable to automotive applications.

Apart from the problems and critical aspects of using hydrogen or methanol as anodic active material, this kind of fuel cell is still far from being applied to the transportation large scale market due to the low efficacy of the Pt based electrocatalyst and to the Pt supply limitations. One way to lower Pt loading is by alloying it with transition metals (Pt–Ni, Pt–Cr, Pt–Fe, Pt–Co, Pt–Cu, etc.). According to the literature [1–4], such alloys show a real enhanced electrocatalytic activity, ascribed to several factors. Interatomic Pt–Pt spacing and the reduction of the coordination number of Pt, increased vacancy of Pt d-orbital, decrease of the surface oxides and subsequent increase of the active Pt sites are all possible explanations indicating that a comprehensive understanding of the reported results has not been achieved yet. Among these alloys, Pt–Co showed the higher electrocatalytic activity [3, 5]. There are several ways of preparing supported Pt–Co alloys. A commonly used method consists of the formation of carbon-supported platinum followed by the deposition of the second metal on Pt/C and alloying at high temperatures [2, 5–9]. The disadvantage of using high temperatures is the metal particle sintering. In order to eliminate this inconvenient other methods of synthesis at low temperatures have been developed [3, 10] but the degree of alloying was poorer.

Mechanochemical synthesis by high energy ball milling is a widespread technique for the preparation of a variety of

metastable materials including nanostructured as well as amorphous and quasi-crystalline phases. The high energy ball milling is suitable for the preparation of high amounts of alloyed phases in a wide range of compositions with a relatively high degree of dispersion [11, 12]. The catalyst can be produced commercially in large scale with consequent lower cost compared to other processes.

In this study, we report on the first results regarding the electrochemical behaviour of nanocrystalline ball-milled Pt–Co alloys as hydrogen fuelled PEMFC electrocatalysts. This preliminary work was centred on improving the electrochemical performances through optimization of the microstructural features. Two Pt–Co catalysts with the nominal composition 20 wt.% alloy (Pt:Co in the molar ratio 0.25:0.75) and C 80 wt.% for the first sample and 20 wt.% alloy (Pt:Co in the molar ratio 0.75:0.25) and C 80 wt.% for the second sample are taken into examination. These two samples are reported in the followings as (20 wt.%)$Pt_{0.25}Co_{0.75}$/C and (20 wt.%)$Pt_{0.75}Co_{0.25}$/C. A 20 wt.% Pt/C catalyst was also prepared. The electrochemical behaviour of the alloy samples were compared with the results obtained by the 20 wt.% Pt/C sample.

2 Experimental

2.1 Mechanochemical synthesis

The preparation of the samples was carried out by high energy ball milling using a SPEX Mixer-Mill Model 8000. This was equipped with a stainless-steel vial of 41.5 mm in height and 15.8 mm in diameter, properly allocated within the larger Spex steel cylinder and fixed in the mill arm. A single sphere of 3.5 g was employed as a milling body. To avoid gaseous contamination, vial charging and sampling were performed in an Argon filled MBraun glove box which maintained oxygen, moisture and nitrogen content below 2 ppm. The ball milling process was conducted in two steps. Firstly, the Pt–Co alloy of the desired composition was obtained by milling 2 grams of the stoichiometric mixture of the pure elements. Afterwards the alloy was milled together with graphite (XC-72 R Vulcan Carbon Black from Cabot), in order to support the Pt–Co powders on C particles. The second step of mechanical treatment was performed on 1 g of powder containing 20 wt.% alloy and 80 wt.% Vulcan Carbon XC-72R.

2.2 Structural analysis

The X-Ray Diffraction (XRD) analyses were carried out using a Bruker D8 diffractometer in the Bragg-Brentano geometry with CuKα radiation ($\lambda = 1.54178$ Å). The patterns were collected in high resolution step scanning mode, in the angular range 30–90° with a step size of 0.05°. The X-ray generator worked at 40 kV and 40 mA, and the goniometer was equipped with a graphite monochromator in the diffracted beam. The quantitative evaluation of phase abundance, average crystallite size and microstructural strain in the powder patterns was performed according to the Rietveld method [13], using the program MAUD [14] running on a personal computer.

Particles morphology and elemental composition were analyzed using a Philips XL-20 scanning electron microscope (SEM) working at 20 kV. SEM pictures were collected at high (HR) and at ultra-high resolution (UHR).

HRTEM analysis was performed on the two Pt–Co alloys supported on carbon using a Jeol JEM 3010 (300 kV) microscope equipped with a side entry and a LaB_6 filament. The powdered samples were ultrasonically dispersed in isopropyl alcohol and the obtained suspension was deposited on a copper grid, coated with a porous carbon film.

2.3 Catalyst ink preparation

A mixture of bi-distilled water, isopropanol (Aldrich) and Nafion (5 wt.%, Electrochem Inc.) was magnetically stirred for 1 h. The ball milled powder catalyst was added and the resulting thicker mixture was further magnetically stirred for 2 h and after that ultrasonicated for 30 min. The catalyst ink obtained was used for the preparation of the cathode in the MEA and for the electrochemical measurements. A similar procedure was followed for the 20 wt.% Pt/C (E-TEK) catalyst ink preparation.

2.4 Electrochemical studies

Electrochemical studies were carried out in both liquid electrolyte (sulphuric acid) half-cell and in PEMFC.

Cyclic voltammetric measurements were conducted in de-aerated electrolyte in 1 M sulphuric acid at room temperature at the scan rate of 10 mV s^{-1} between ± 0.7 V vs. Hg/Hg_2SO_4 reference electrode. The counter electrode was a piece of Pt grid. 5 μL of the catalyst ink has been deposited on a glassy carbon Rotating Disk Electrode (RDE). The rotation speed of the RDE electrode was set at 900 rpm during the measurements. The cell was purged with Argon for 1 h prior to the measurements. A VoltaLab PGZ301 Radiometer Analytical was employed to run the measurements. The electrochemical active surface (EAS) area was determined through the evaluation of the Coulombic charge (Q_H) for hydrogen desorption during a cyclic linear scan voltammetry:

$$EAS = Q_H/([Pt] \times 210)$$

where [Pt] was the platinum loading on the electrode (mg cm^{-2}), Q_H the charge for hydrogen desorption

(mC cm^{-2}) and 210 μC cm^{-2} represented the charge required to oxidize a monolayer of hydrogen on bright platinum [15, 16].

The electrocatalyst performance in a real cell was obtained by assembling MEAs with the considered sample at the cathode. The electrodes were prepared by the painting deposition technique of the ink catalyst on the LT 1200-W E-TEK ELAT GDL (gas diffusion layer). In order to observe the effect of Co on the Pt performances, Pt loading was 0.5 mg cm^{-2} on both anode and cathode for all samples. The Nafion content in the catalyst ink was 33 wt.% with respect to the metal loading. The MEA was obtained by the *sandwich* hot pressing of the electrodes on a Nafion 115 membrane at 35 kg cm^{-2} and 393 K for 2 min by a DGTS press PM20 04799C. The so prepared MEAs were tested in a single 5 cm^2 PEMFC (Electrochem Inc., code number E3974) having an electrode area of 5 cm^2. The anode and cathode feed were high purity hydrogen and oxygen respectively. The cell temperature was kept constant at 343 K. The fuels were humidified at a relative humidity (RH) of 80%. Polarization curves of the membrane electrode assemblies (MEAs) were traced by using a PC driven ET electronic load mod. ELP/SL400. Starting from the open circuit potential, the current was modified at a rate of 10 mA s^{-1} until a cell potential of 0.3 V was reached.

3 Results and discussion

3.1 Structural characterization

The mechanical alloying process of Pt–Co mixtures was followed by XRD analyses, and selected patterns relevant to both the alloy compositions are reported in Fig. 1, as a function of times of mechanical treatment.

Irrespective of the stoichiometry of the starting mixtures, the mechanical processing was effective in promoting the formation of solid solutions soon after few minutes. The quantitative analysis indicated that the fcc allotrope of cobalt appeared to be involved preferentially in the early stage of alloying reaction, through its dissolution within fcc Pt, while the subsequent evolution was dependent on the mixture stoichiometry.

The fcc sequence of peaks was evident in the patterns of both samples. However, while in the case of $Pt_{75}Co_{25}$ composition the alloying proceeds with the formation of a single disordered Pt-rich solid solution, whose lattice parameter was about 3.86 Å, conversely in the $Pt_{25}Co_{75}$ composition, a different reaction path seemed to occur. The Pt-rich solid solution formed in the first stages of milling, evolved as a consequence of the alloying with the Co matrix, to a new fcc phase, with shorter lattice parameter (3.68 Å), Co-rich solid solution. This is supported by the systematic simultaneous presence of bicomponent solid solution in the pattern relevant to the sample milled for 20 h. Further milling converted the structure to a single Co-rich fcc solution. The considerable line broadening of peaks was ascribed to the effects of finite size of coherent diffraction domains and to microstrain. For the $Pt_{75}Co_{25}$ composition, the average crystallite size was ca 200 (±10) Å after 8 h, when the lattice microstrain was also maximum, but a further mechanical treatment tended to increase the average crystal size value, up to 260 (±10) Å and to decrease the strain up to the value of 4.5×10^{-3} relevant to the sample milled 21 h shown in Fig. 1a. The average crystallite size for the $Pt_{25}Co_{75}$ composition in the fcc major phase was of 150 Å, while in the tested specimen, treated up to 30 h, its domain size increased to 198 (±0) Å.

The SEM images, reported in Fig. 2, showed that both (20 wt.%)$Pt_{0.25}Co_{0.75}$/C and (20 wt.%)$Pt_{0.75}Co_{0.25}$/C electrocatalysts have porous structures, with a broad distribution of particles size. EDS analysis (data not shown) evidenced some regions with small alloy particles of 3–7 nm surrounding the C particles, while there are other regions, also

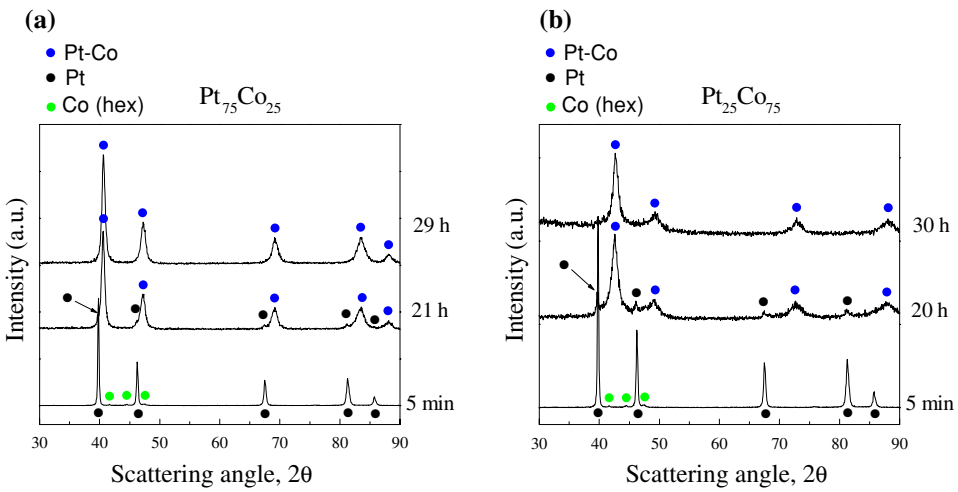

Fig. 1 X-ray diffraction pattern of the Pt–Co nanocatalyst compositions **a** $Pt_{75}Co_{25}$ and **b** $Pt_{25}Co_{75}$

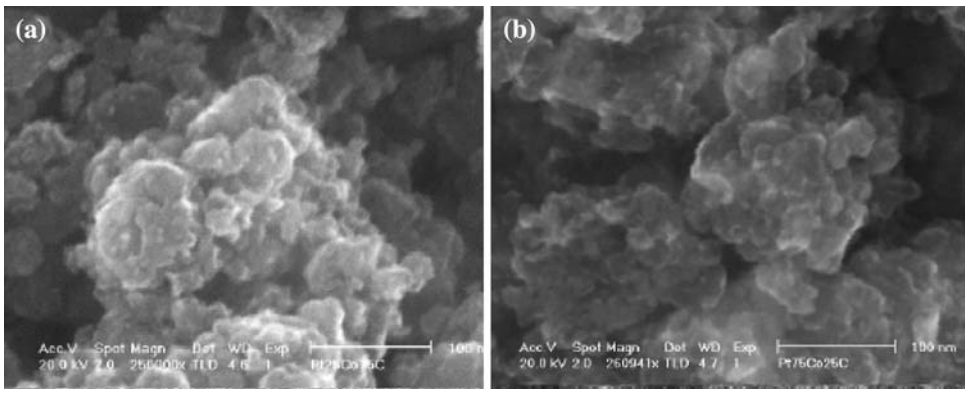

Fig. 2 SEM images of **a** (20 wt.%)$Pt_{0.25}Co_{0.75}$/C and **b** (20 wt.%)$Pt_{0.75}Co_{0.25}$/C. Both images were taken at 260000× magnification

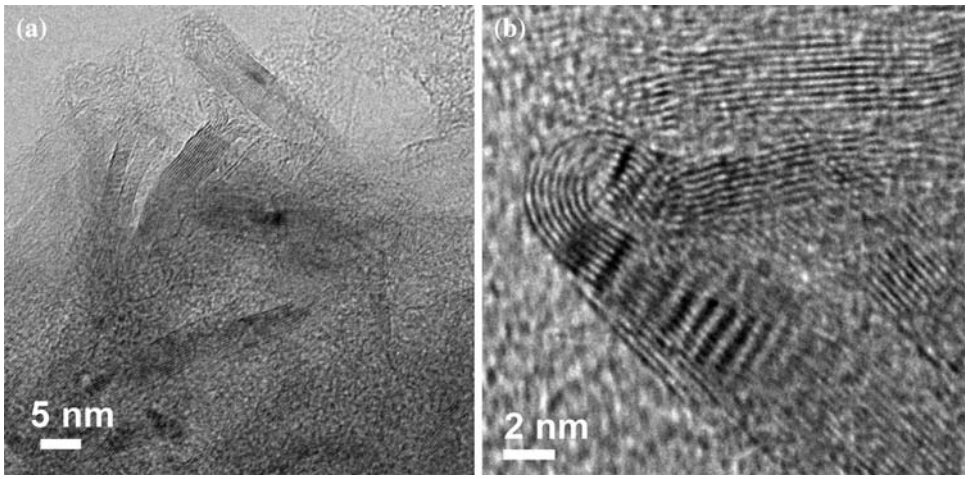

Fig. 3 HRTEM image of (20 wt.%)$Pt_{0.25}Co_{0.75}$/C (**a**). Detail showing a loop of graphite sheet (**b**). The images were taken at an original magnification of 300000× and 800000×, respectively

observed by HRTEM as will be discussed later, with alloy particles even larger than graphite. These features were due to the mechanical treatment effect.

HRTEM analysis was performed on the (20 wt.%)$Pt_{0.25}Co_{0.75}$/C and (20 wt.%)$Pt_{0.75}Co_{0.25}$/C samples. The images are shown in Figs. 3 and 4, respectively. The milling procedures performed to prepare the Pt–Co alloy and then the final supported samples induced a deep morphological modification on the carbon in both samples. In particular, the agglomerates of globular, round shaped carbon particles with amorphous structure of Vulcan XC-72R turned into a graphitic material [17], where the high energy ball milling has provoked an exfoliation process and the bending of graphite sheets themselves (Fig. 3a). Moreover, the curved stacks of graphite sheets can form loops, here shown in Fig. 3b. Touzik et al. studied the structural transformations in high purity graphite upon high energy ball milling under Ar and H_2 atmosphere by BET and HRTEM measurements and observed very similar features [18]. In our case, a role of the cobalt on the final porosity of the material cannot be excluded, since at high temperature Co can induce tunnelling processes [19], hence possibly also during a high-energy ball-milling procedure. Finally, the observation of metallic alloy PtCo particles was very difficult on the (20 wt.%)$Pt_{0.25}Co_{0.75}$/C sample, possibly due to the disordered morphology of the graphitic support and to the high dispersion of the metallic phase.

On the contrary, on the (20 wt.%)$Pt_{0.75}Co_{0.25}$/C sample, small agglomerates of metallic particles of size around 5 nm were observed (Fig. 4).

3.2 Electrochemical measurements

The first electrochemical tests on (20 wt.%)$Pt_{0.25}Co_{0.75}$/C and (20 wt.%)$Pt_{0.75}Co_{0.25}$/C samples aimed at determining the electrochemically active surface (EAS) area. Both samples did not present any electrochemical activity at the first cycle, as can be seen from Fig. 5a, b. The curves showed only non faradaic current with no peak indicating electrochemical process. The curve related to the (20 wt.%) $Pt_{0.75}Co_{0.25}$/C sample (Fig. 5a) changes until the 300th cycle and took the typical shape of an active catalyst. In the case of the (20 wt.%)$Pt_{0.25}Co_{0.75}$/C sample, there was no activation via repeated voltammetric cycles (Fig. 5b). The difference in the behaviour of the alloys samples is related to the different composition of the electrodes that is calculated for 5 μL of sample (Table 1). Carbon and Nafion can partly hinder Pt from the electrolyte and isolate it so causing the

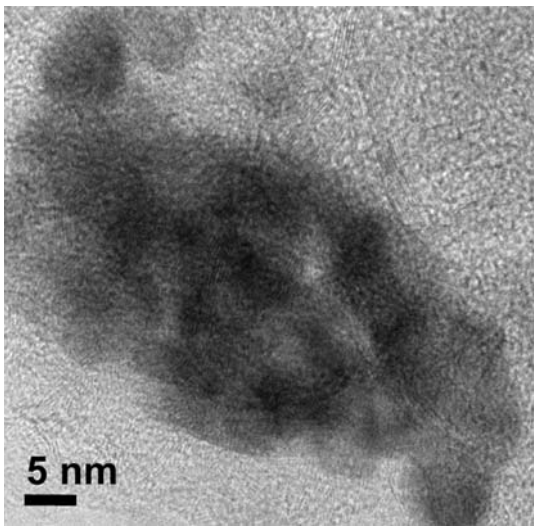

Fig. 4 HRTEM images of (20 wt.%)$Pt_{0.75}Co_{0.25}$/C. The image was taken at an original magnification of 400000×

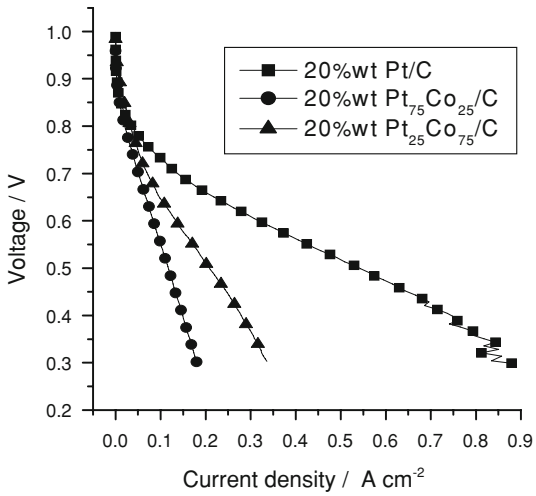

Fig. 6 Polarization curves of the considered alloy samples and a standard pure Pt sample

behaviour reported in Fig. 5b, as suggested by the high values of the C/Pt and Nf/Pt ratios for the (20 wt.%) $Pt_{0.25}Co_{0.75}$/C sample reported in Table 1.

Therefore, it has been possible to calculate the EAS value only for one of our samples (Table 1). HRTEM results can justify this feature, considering that on this sample metal particles agglomerates have been observed (Fig. 4). The similar composition in platinum, carbon and Nafion (summarised in Table 1) cannot explain the fact that, while the standard catalyst shows its best curve within the first 10 cycles, the (20 wt.%)$Pt_{0.75}Co_{0.25}$/C sample needs 300 cycles to be activated. One hypothesis may connect this difference in behaviour to the different way of synthesising the alloy sample and Pt sample. It also seems logical to relate this behaviour to the presence of Co though it is not well clear, from these preliminary data, how the metal interacts.

Preliminary results on the performance of the Pt–Co composite catalysts are shown in Fig. 6, where the polarization curve relevant to a MEA with the cathode prepared with a commercial Pt/C powder electrocatalyst is reported for comparison. The curve for the sample 20 wt.% Pt/C (Fig. 6) clearly reports all the features to be found in this kind of test. A fast voltage loss which is typical of a slow electrode reaction like oxygen reduction appeared initially,

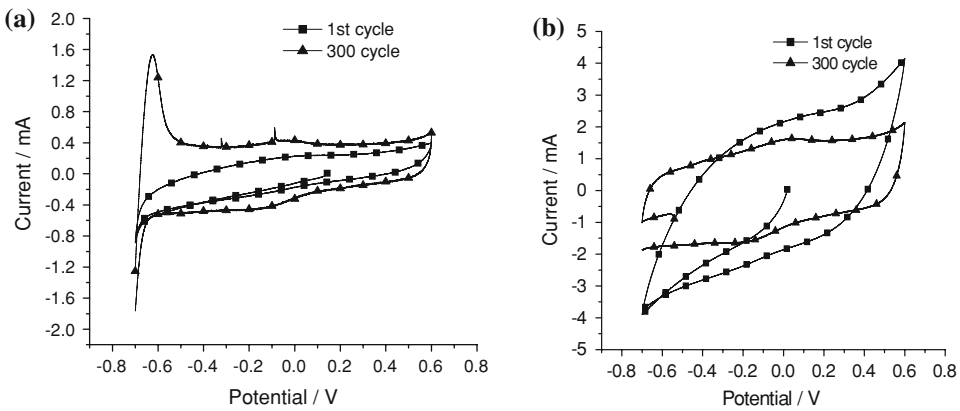

Fig. 5 Voltammograms for (**a**) (20 wt.%)$Pt_{0.75}Co_{0.25}$/C and (**b**) (20 wt.%)$Pt_{0.25}Co_{0.75}$/C in 1 M H_2SO_4 purged with N_2 at room temperature at a sweep rate of 20 mVs^{-1}

Table 1 Composition of the ink samples (5 μL) deposited on the working electrode in the CV tests

Sample	Pt mg cm^{-2}	Co mg cm^{-2}	C mg cm^{-2}	Nafion mg cm^{-2}	C/Pt	Nf/Pt	Pt/Co	EAS m^2 g^{-1}
(20 wt.%)$Pt_{0.75}Co_{0.25}$/C	0.70	0.07	3.04	1.88	4.34	2.69	10.1	102
(20 wt.%)$Pt_{0.25}Co_{0.75}$/C	0.40	0.36	3.08	1.89	7.70	4.72	1.1	–
Pt 20 wt.%	0.80	–	3.2	1.97	4.00	2.46		161

followed by a linear less steep decrease due to the internal ohmic resistance of the cell. The limited diffusion rate of the reactants to the reaction sites drawn to the final increase of the curve slope. In the case of (20 wt.%)$Pt_{0.75}Co_{0.25}$/C and (20 wt.%)$Pt_{0.25}Co_{0.75}$/C samples, the high increase of the curve slope may be due to the presence of a highly porous material in which the pores can be formed by curved stacks of graphite sheets as evidenced by HRTEM analysis (see Fig. 3b).

The catalysts activity in a fuel cell, as reported in Fig. 6, was very poor with respect to the standard. The cause resides in the material and/or in the catalyst preparation and dispersion method, being the MEAs prepared and tested in the same conditions. Using a logarithmic scale for the initial part of the curve (Fig. 7), it becomes clear that though the overall poor performance, the (20 wt.%) $Pt_{25}Co_{75}$ sample was, at least at low currents, more active. Also, it appears clear from the lines slope that the very high internal resistance exerted a marked influence on the MEA performance and we suppose that was the major component of the potential loss.

We verified the above supposition by analysing the previous data with an electrochemically oriented mathematical model described elsewhere [20]. a, b, c, d lines in Fig. 8 gave the various polarization terms in an incremental form. In other words, this model allows to separate the contributions of the various energetic losses. The overpotential terms taken into account in this model are: activation overpotentials, concentration overpotentials and ohmic losses.

In particular:

- curve a was the computed curve for the activation overpotential of the oxygen reduction reaction;
- curve b was the sum of the activation overpotentials of the oxygen reduction and hydrogen reduction reactions;

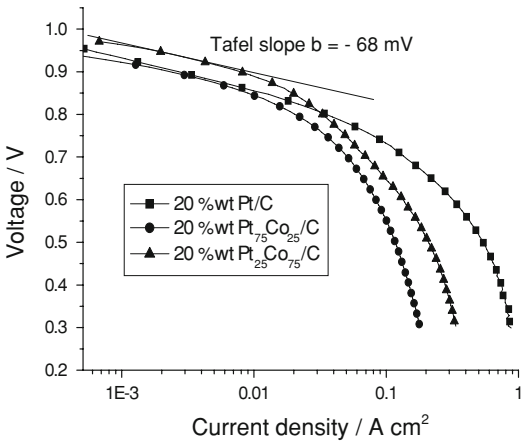

Fig. 7 Polarization curves of the considered alloy samples and a standard pure Pt sample on logarithmic scale

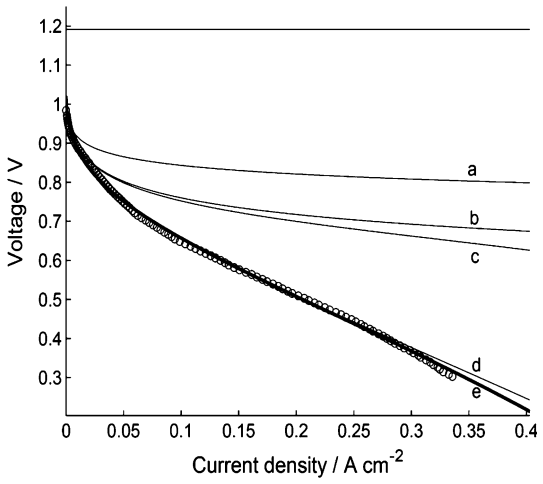

Fig. 8 Analysis of the polarization curve corresponding to (20 wt.%)$Pt_{0.75}Co_{0.25}$/C sample

- curve c was the sum of the activation and concentration overpotentials of the oxygen reduction and hydrogen reduction reactions;
- curve d added to the sum calculated for the curve c, represented the value of the ohmic drop due to resistance of the membrane and electrodes. In the total curve e, the ohmic resistance term depending on the current intensity was included.

The contribution of the resistance term to the potential loss was very high and consistent with our supposition, as evidenced by curve d.

Comparing the performances of the two alloy catalysts, it appeared puzzling that the sample with an immeasurable EAS [(20 wt.%)$Pt_{0.25}Co_{0.75}$/C] behaved better than the apparently electrochemically active one [(20 wt.%)$Pt_{0.75}Co_{0.25}$/C]. A possible explanation can be found in the values reported in Table 2. In the cell cathodes, the loading of Pt was the same in all samples, but the total amount of C and Nafion was different. Moreover, the Nafion ionomer does not only exert a binding action, but also allows the proton motion from the membrane to the catalyst grains. The (20 wt.%)$Pt_{0.25}Co_{0.75}$/C ink had a higher quantity of ionomer that increased the flow of protons with respect to the (20 wt.%)$Pt_{0.75}Co_{0.25}$/C sample (Fig. 6). We ascribed the better performance of (20 wt.%)$Pt_{0.25}Co_{0.75}$/C electrodes to this characteristic.

By comparing the values and the ratios for (20 wt.%) $Pt_{0.75}Co_{0.25}$/C and 20 wt.% Pt/C (Table 2) we saw that the figures are quite similar. As in the case of cyclic voltammetry measurements, the differences between the performances of these two samples may be related to the presence of the Co and/or to the method of synthesis.

Performances are usually considered not only dependent on the catalyst particles size [21] but also on the

Table 2 Composition of the positive electrodes of the test fuel cells

Sample	Pt mg cm^{-2}	Co mg cm^{-2}	C mg cm^{-2}	Nafion mg cm^{-2}	C/Pt	Nf/Pt	Pt/Co
(20 wt.%)$Pt_{0.75}Co_{0.25}$/C	0.50	0.05	2.20	1.35	4.40	2.70	10.1
(20 wt.%)$Pt_{0.25}Co_{0.75}$/C	0.50	0.45	3.81	2.34	7.62	4.68	1.1
Pt 20 wt.%	0.50	–	2.00	1.23	4.00	2.46	

inhomogeneous bimetallic particle size distribution with a fraction of large particles (up to 50 nm) [16] that reduce the active area of the catalyst and induce the electrically insulation and hence not taking part to the electrochemical tests. Moreover, the increase in Co content in the alloy, varying the electronic density available for adsorption and reducing the average metal–metal bond length, seemed responsible of the OH adsorption decrease as well as of the better H sorptive qualities on the alloy surface. Furthermore the small amount of unalloyed Pt, or Pt-rich alloy may have an active role in improving the catalyst activity for the oxygen reduction process, by itself or with the synergic effect due to the bimetallic Co-rich matrix.

4 Conclusions

The mechanochemical synthesis proved to be a suitable preparation technique for electrochemically active alloys. The fitting procedure of the initial part of the polarization curves with an electrochemical model revealed a lower activation overpotential in the case of the alloys. The electrocatalytic efficacy of the present samples was definitely lower than the standard Pt sample. The main reason seems to reside in the dispersion of Pt, Co and Nafion particles obtained by mechanical milling. Also, the lower performances of the alloy catalysts are related to the C/Pt and Nf/Pt ratios that are not optimized for the alloy samples. A further improvement in synthesis route and strategy could be reached by taking into account the specific milling dynamic parameters as well as evaluating proper impact energy and milling intensity values.

Acknowledgements The Italian Regione Piemonte Council (research project C104) contributed in financing the present research. The authors are grateful to Prof. P. Spinelli (Politecnico di Torino) for the mathematical interpretation of the experimental results. A special acknowledgment is for Gabriele Mulas (Università di Sassari) for all his work on mechanical milling. Prof. N. Penazzi (Politecnico di Torino) is gratefully acknowledged for the helpful discussions and support.

References

1. Salgado JRC, Antolini E, Gonzalez ER (2005) J Power Sources 141:13
2. Salgado JRC, Antolini E, Gonzalez ER (2004) J Phys Chem B 108:17767
3. Xiong L, Kannan AM, Manthiram A (2002) Electrochem Commun 4:898
4. Antolini E, Salgado JRC, Gonzalez ER (2006) Appl Catal B Environ 63:137
5. Shukla AK, Neergat M, Bera P, Jayaram V, Hegde MS (2001) J Electroanal Chem 504:111
6. Beard BC, Ross PN (1990) J Electrochem Soc 137:3368
7. Min M, Cho J, Cho K, Kim H (2000) Electrochim Acta 45:4211
8. Oliveira Neto A, Perez J, Gonzalez ER, Ticianelli EA (1999) J New Mater Electrochem Syst 2:189
9. Sirk AHC, Campbell SA, Birss VI, Soderberg JN (2005) J Electrochem Soc 152:2017
10. Xiong L, Manthiram A (2005) Electrochim Acta 50:2323
11. Schwarz RB, Petrich RR, Saw CK (1985) J Non Cryst Solids 76:281
12. Cocco G, Enzo S, Schiffini L, Battezzati L (1988) Mater Sci Eng 97:43
13. Lutterotti L, Ceccato R, Dal Maschio R, Pagani E (1998) Mater Sci Forum 278–281:87
14. Cannas C, Musinu A, Piccaluga G, Deidda C, Serra F, Bazzoni M, Enzo S (2005) J Solid State Chem 178:1526
15. Merzougui B, Swathirajan S (2006) J Electrochem Soc 153:A2220
16. Perez J, Gonzalez ER, Ticianelli EA (1998) Electrochim Acta 44:1329
17. Bayrakceken A, Smirnova A, Kitkamthorn U, Aindow M, Türker L (2008) J Power Sources 179:532
18. Touzik A, Hentsche M, Wzel R, Hermann H (2006) J Alloy Comp 421:141
19. Manzoli M, Boccuzzi F (2003) J Power Sources 118:304
20. Spinelli P, Francia C, Ambrosio EP, Lucariello M (2008) J Power Sources 178:517
21. Bazzoni M, Bettinelli M, Daldosso M, Enzo S, Serra F, Speghini A (2005) J Solid State Chem 178:301